CALIBRATION OF C-ARM FOR ORTHOPEDIC INTERVENTIONS VIA STATISTICAL MODEL-BASED DISTORTION CORRECTION AND ROBUST PHANTOM DETECTION

Steffen Schumann, Xiao Dong, Marc Puls, Lutz-Peter Nolte, Guoyan Zheng

Institute for Surgical Technology and Biomechanics, University of Bern, Switzerland

ABSTRACT

In this paper, we present a novel C-arm calibration approach for orthopedic applications that is based on a distortion correction plate with fiducials arranged in a single-plane and a novel mobile phantom. The former is designed to be rigidly attached to the image intensifier and is used together with a statistical model of the geometrical image distortion pattern for intra-operative image distortion correction. The latter can be placed to anywhere close to the patient anatomy being imaged. A simulation based method is then proposed for a robust detection of the phantom from an intra-operatively acquired image in order to compute both the intrinsic and the extrinsic parameters of the acquired image. Validation study performed on 20 cadaver images demonstrated an average calibration accuracy of 0.8 ± 0.4 mm.

***Index Terms*—** X-rays, calibration, orthopedic procedures

1. INTRODUCTION

The fluoroscope, also known as C-arm due to its "C" shape, is often used intra-operatively in orthopedics for visualizing underlying anatomy and surgical instruments. Though its applications in interventional disciplines are pervasive, its disadvantages are also apparent. A fluoroscopy image is a two-dimensional (2D) projection image, which lacks depth information. The image is distorted and has limited field of view. Its ability in providing three-dimensional (3D) quantitative information is limited and its application involves high radiations to the interventional team. This has lead to the development of methods for precise C-arm calibration (there are plenty of papers in the literature about C-arm calibration, see [1] for an example), which are important for various fluoroscopy image based applications. The goal of the calibration is to correct the geometric image distortion and to estimate the C-arm projection parameters. For this purpose, a cage with fiducials arranged in multi-planes is normally required to be attached to the image intensifier, which has the disadvantage of interfering with the patient anatomy being imaged and requires tracking of C-arm machine by an external tracker, which sometimes is judged to be too cumbersome.

There exist attempts to replace the external tracker with a mobile phantom. Yao et al. [3] proposed to use a line fiducial based phantom mounted on a robot's tool holder to register the end effector of the surgical robot to a C-arm image. Inspired by this work, Jain and Fichtinger [4] developed a new phantom that used ellipses and straight lines as fiducials in addition to points. Although encouraging results were presented with this new phantom [4], it was recently reported by Otake et al. [5] that automatic segmentation of this phantom from an intra-operatively acquired image was not always possible due to severe background clutter. They thus proposed to use a manually initialized, model-based iterative 2D-3D registration for an accurate detection of the phantom from the image.

Attempts to characterize the C-arm distortion with a statistical framework have previously been done by Chintalapani et al. [2]. Based on a statistical model of the geometrical image distortion, Chintalapani et al. discussed using fewer fiducials [2] as a fiducial for distortion correction. Although it is feasible to combine this statistical framework with one of the mobile phantoms mentioned above, there has no such work reported until now.

2. MATERIALS AND METHODS

2.1. Statistical model based image distortion correction

2.1.1. Image Distortion Correction Plate

To build a statistical model of the C-arm image distortion pattern and to use it for the later image distortion correction, we designed a new image distortion calibration plate with embedded fiducials as shown in the left column of Fig. 1, where the central part of the plate is detachable. The same plate is used in two different stages as follows.

- Off-line statistical model building stage. This stage is only needed to be done off-line one time for a C-arm. At this stage, the central part of the plate will be mounted to have a complete plate (see top image, left column of Fig.1) and the complete plate will be rigidly attached to the image intensifier. By placing the C-arm in different orientations and acquiring images of the plate, we can establish a statistical model of the C-arm image distortion pattern from fiducial projections

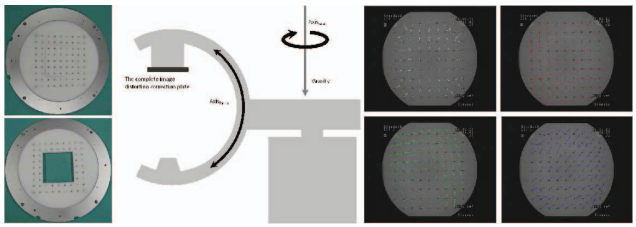


Fig. 1. Left column: the image distortion plate; middle column: the setup for acquisition of images for building the statistical model of the C-arm image distortion pattern; right column: statistical model of the C-arm image distortion pattern, i.e., the mean displacement map (top left) and the first three eigen displacement maps (top right: 1^{st}; bottom left: 2^{nd}, bottom right: 3^{rd}).

detected from all acquired images (see below for details).

- On-line intra-operative image calibration stage. At this stage, the central part of the plate will be detached to have a plate with hole (see bottom image, left column of Fig.1) and the plate will then be rigidly attached to the image intensifier. As only the sparse fiducials around the border of the plate are visible in each intra-operatively acquired image, the detected boundary fiducial projections are combined with the statistical model of the image distortion pattern to estimate the projection locations of those missing fiducials for image distortion correction (see below for details).

2.1.2. Statistical model of the C-arm image distortion pattern

The statistical model of the C-arm image distortion pattern is constructed off-line from images of the complete plate (Fig.1, left) acquired at different imaging positions. The complete plate has totally 77 cross-shaped fiducials. The imaging positions are selected by rotating the C-arm around two axes $Axis_{Grav}$ and $Axis_{Pinch}$ while keeping the roll angle of the C-arm at 0 degree as shown in the middle column of Fig. 1. The first rotation Rot_{Grav} is around the gravity direction, i.e. rotating the whole C-arm machine horizontally to reveal the influence of the magnetic field of the earth, and the sampling interval is 20 degrees. The second rotation is the pinch rotation of the C-arm and the sampling interval is also 20 degrees. We additionally acquired three images resulting in 383 calibration images in total.

Given the model building images $\{I^n\}, n = 1, 2, ..., N = 383$, a cross-correlation based template matching is used to detect the projections of all the fiducials from each image I^n and the detected fiducial positions $\{\mathbf{P}_n^i\}; i = 1, 2, ..., 77, n = 1, 2, ..., 383$, are saved for the model building.

The statistical model is built as follows:

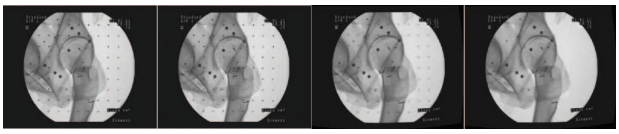


Fig. 2. Statistical model based image distortion correction, from left to right: detection of boundary fiducial projection, instantiation of the statistical model of the C-arm image distortion pattern, image undistortion, and fiducial projection inpainting.

Distortion vector computation For each model building image I^n, we compute the displacement vector $\mathbf{D}_n = [D_{n,x}^1, D_{n,y}^1, ..., D_{n,x}^{77}, D_{n,y}^{77}]^T$, where $D_n^i = [D_{n,x}^i D_{n,y}^i]^T$ are defined as the vectors starting from the ideal/nominal fiducial projections, $\overline{\mathbf{P}}^i$, which are determined from the physical geometry of the fiducial layout, to the detected fiducial projection $\mathbf{P}_n^i$.

PCA modeling of the displacement field Taking the displacement vectors $\{\mathbf{D_n}\}$, $n = 1, 2, ..., 383$ as the input, we first compute the mean displacement map $\mathbf{M}_D$ as the average of all displacement vectors. The mean displacement map is then subtracted from each displacement vector before we apply principal component analysis to compute the eigen displacement maps $\{\mathbf{P}_D^i\}$ and the eigen values $\{\lambda^i\}$ of the variation. Then, any displacement map can be parameterized by the statistical model with much less number of parameters.

2.1.3. Image distortion correction

Intra-operatively, the central part of the image distortion correction plate will be removed before it is attached to the image intensifier. Thus, only the boundary fiducials will be visible in an intra-operatively acquired image. The projections of these boundary fiducials can be robustly detected by using the same cross-correlation based template matching as we mentioned before such that the displacement vectors of these fiducials with respect to the corresponding nominal fiducial projections can be precisely estimated. The estimated displacement vectors of these boundary fiducials are then used to instantiate the statistical model of the C-arm image distortion pattern, leading to the extrapolation of the displacement vectors for those missing fiducials at the central part of the plate. In this work, the extrapolation is done based on the statistical instantiation method proposed by Rajamani et al. [6]. Based on the displacement vectors of all fiducials, the image is then undistorted using a fifth order polynomial-based approach. Moreover, the fiducial projections are inpainted from the image with the method implemented in OpenCV library. Fig. 2 shows an example of statistical model based image distortion correction.

2.2. Phantom design and image calibration

In this step, we need to compute both the intrinsic and the extrinsic parameters of the image. This is achieved in our approach by developing a mobile phantom as shown in the left column of Fig.3. There are totally 16 sphere-shaped fiducials embedded in this phantom: 7 big fiducials with diameter of 5.0 mm and 9 small fiducials with diameter of 2.5 mm. The 16 fiducials are arranged in three different planes: all 7 big fiducials placed in one plane and the rest 9 small fiducials distributed in other two planes. Furthermore, the 7 big fiducials are arranged to form three line patterns as shown in Fig.3, left. Every line pattern consists of three fiducials $\{M_i^1, M_i^2, M_i^3\}, i = 1, 2, 3$ with different ratios $\{r_i = |M_i^1 M_i^2|/|M_i^2 M_i^3|\}$. The exact ratio for each line is used below to identify which line pattern has been successfully detected.

After the distortion of an intra-operatively acquired image is corrected, we apply a sequence of image processing operations to the image. As those fiducials are made from steel, a simple threshold-based method is first used to segment the image. Connected-component labeling is then applied to the binary image to extract a set of separated regions. Morphology analysis is further applied to each label connected-component to extract two types of regions: candidate regions from big fiducial projections and candidate regions from small fiducial projections. The centers of these candidate regions are regarded as projections of the center of a potential fiducial. Due to background clutter, it is feasible that some of the candidate projections are outliers and that we may miss some of the true fiducial projections. Furthermore, to calculate both the intrinsic and the extrinsic parameters, we have to detect the phantom from the image. Here phantom detection means to establish the correspondences between the detected 2D fiducial projection centers and their associated 3D coordinates in the local coordinate system of the phantom. For this purpose, a robust simulation-based method as follows is proposed. The pre-condition to use this method to build the correspondences is that one of the three line patterns has been successfully detected. Due to the fact that these line patterns are defined by big fiducials, chance to missing all three line patterns is rare.

We model the C-arm projection using a pin-hole camera.

$$\alpha[I_x, I_y, 1]^T = \mathbf{K}(\mathbf{R}[x, y, z]^T + \mathbf{T}) = \mathbf{P}[x, y, z, 1]^T \quad (1)$$

where α is the scaling factor, $\mathbf{K}$ is the intrinsic calibration matrix, $\mathbf{R}$ and $\mathbf{T}$ are the extrinsic rotation matrix and translational vector, respectively. Both the intrinsic and the extrinsic projection parameters can be combined into a 3-by-4 projection matrix $\mathbf{P}$ in the local coordinate system established on the mobile phantom.

The idea behind the simulation-based method is to do a pre-calibration to compute both the intrinsic matrix $\mathbf{K}$ as well as the extrinsic parameters $\mathbf{R}_0$ and $\mathbf{T}_0$ of the C-arm in a reference position (see the middle column of Fig.3 for a schematic view of the reference position). Then, assuming that the intrinsic matrix $\mathbf{K}$ is not changed from one image to another (we only use this assumption for building the correspodences), the projection of the C-arm at any other position with respect to the phantom can be expressed as

$$\alpha[I_x, I_y, 1]^T = \mathbf{K}(\mathbf{R}_0(\mathbf{R}^x\mathbf{R}^y\mathbf{R}^z[x, y, z]^T + \mathbf{T}) + \mathbf{T}_0) \quad (2)$$

where $\mathbf{R}^x$, $\mathbf{R}^y$, $\mathbf{R}^z$ and $\mathbf{T}$ are the rotation matrices around three axes (assuming the z-axis is in parallel with the view direction of the C-arm at the reference position, see the middle column of Fig.3 for details) and the translation vector from an arbitrary acquisition position to the reference position, respectively, expressed in the local coordinate of the mobile phantom. To detect the phantom projection when the C-arm is placed in the new position, the simulation-based method consists of two steps.

Image normalization. The purpose of this step is to get rid of the influence of the parameters $\mathbf{R}^z$, α, and $\mathbf{T}$ on the phantom detection by normalizing the image acquired at the new position as follows. Assuming that we know the correspondences of fiducials on one line pattern, which is defined by 3 landmarks M_1, M_2, M_3 with their correspondent projections at IM_1, IM_2, IM_3, we can define a 2D coordinate system based on IM_1, IM_2, IM_3, whose origin O is located at $(IM_1 + IM_2)/2$ and the x-axis is defined along the direction $O \rightarrow IM_3$. Accordingly a 2D affine transformation $T_{normalize}$ can be computed to transform this line pattern based coordinate system to a standard 2D coordinate system with its origin at (0, 0) and x-axis along direction (1, 0) and at the same time to normalize the length of the vector $IM_1 \rightarrow IM_3$ to 1. By applying $T_{normalize}$ to all the fiducial projections, it can be observed that for a pair of fixed $\mathbf{R}^x$ and $\mathbf{R}^y$, we can get the same normalized image no matter how the other parameters $\mathbf{R}^z$, α, and $\mathbf{T}$ are changed because the influence of these parameters is just to translate, rotate, and scale the fiducial projections, which can be compensated by the normalization operation. Therefore, the fiducial projections after the normalization will only depend on the rotational matrices $\mathbf{R}^x$ and $\mathbf{R}^y$.

Normalized image based correspondence establishment. Since the distribution of the fiducial projections in the normalized image only depends on the rotation matrices $\mathbf{R}^x$ and $\mathbf{R}^y$, it is natural to build a look-up table which up to a certain precision (e.g., 1^o) contains all the normalized fiducial projections with different combination of $\mathbf{R}^x$ and $\mathbf{R}^y$. This is done off-line by simulating the projection operation using Eq. (2) based on the pre-calibrated projection model of the C-arm at the reference position. For an image acquired at position other than the reference, we apply the normalization operation as described above to all the detected candidate fiducial projections. The normalized candidate fiducial pro-

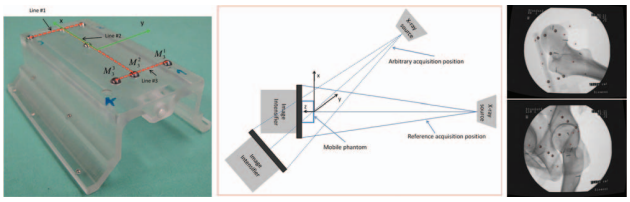


Fig. 3. Fluroscope tracking phantom (left), schematic view of the look-up table based method for 2D-3D correspondences (middle), and two examples of phantom detection (right).

jections are then compared to those in the look-up table to find the best match. Since the items in the look-up table are generated by a simulation procedure, we know exactly the correspondence between the 2D fiducial projections and their corresponding 3D coordinates. Therefore, we can establish the correspondences between the candidate fiducial projections and the fiducials embedded in the phantom. See the right column of Fig.3 for two examples of the phantom detection.

As soon as the correspondences are established, we can further fine-tune the fiducial projection location by applying a cross-correlation based template matching. After that, the direct linear transformation algorithm [7] is used to compute the projection matrix $\mathbf{P}$.

3. EXPERIMENTS AND RESULTS

To evaluate the efficacy of the proposed approach, we conducted following three experiments on a Siemens Siremobile IsoC-3D C-arm machine (Siemens Medical Solutions, Erlangen, Germany).

Statistical model based image distortion correction. In this experiment, we acquired 9 cadaver images of the complete plate by placing the C-arm in different locations with different orientations. The fiducial locations estimated by the statistical model based method were compared to those obtained by direct image detection. A mean error of 1.6 ± 1.8 pixels was found, which leading to an image distortion correction error of 0.6 ± 0.7 pixels.

Single image calibration accuracy. In this experiment, we acquired 10 pairs of images of cadavers using the plate with hole and the mobile phantom by placing the C-arm to different orientations. To evaluate the accuracy of the C-arm calibration with the proposed approach, we attached optoelectronically trackable markers to both the cadaver femur and the mobile phantom. We then implanted five screws into the cadaver femur and performed a pointer-based digitization to get the 3D coordinates of the screw head centers. After the calibration of each image, the calibration accuracy was evaluated by computing the distance between the digitized center of each screw head and its back-projection line emitted from the center of the screw head projection to the X-ray focal point. For all 20 images, we can successfully detect the phantom. A mean calibration accuracy of 0.8 ± 0.4 mm (min = 0.0 mm and max = 2.0 mm) was found.

Biplanar image reconstruction accuracy. The same 10 pairs of C-arm images as used in the last experiment were used in this experiment. The 3D coordinate of the screw head centers used in the last experiment was also used in this experiment as the ground truth. Each time, the two projections of one screw head in one pair of images were used to reconstruct the location of its center. The image-based reconstruction was then compared to the pointer-based digitization to evaluate the biplanar reconstruction accuracy. An average reconstruction accuracy of 0.8 ± 0.3 mm (min = 0.2 mm and max = 1.7 mm) was found.

4. CONCLUSIONS

In this paper, we proposed a novel C-arm calibration approach that was based on a distortion correction plate with fiducials arranged in a single-plane and a novel mobile phantom. We developed a statistical model based method for image distortion correction and a simulation-based method for robust phantom detection. The expriment results demonstrated the efficacy of the proposed approach.

5. REFERENCES

[1] R. Hofstetter, et al.: Fluoroscopy as an imaging means for computer assisted surgical navigation. Computer Aided Surgery **4** (1999) 65–76.

[2] G. Chintalapani, A., Jain, R., Taylor: Statistical characterization of C-arm distortion with application to intraoperative distortion correction. SPIE Medical Imaging 2007, Vol. **6509** (2007) 65092Y.1–65092Y.8.

[3] J. Yao, et al.: A C-arm fluoroscopy-guided progressive cut refinement strategy using a surgical robot. Computer Aided Surgery **5** (2000) 373–390.

[4] A., Jain, and G., Fichtinger: C-arm tracking and reconstruction without an external tracker. MICCAI'06, LNCS **4190** (2006) 494–502.

[5] Y., Otake, et al.: An iterative framework for improving the accuracy of intraoperative intensity-based 2D/3D registration for image-guided orthopedic surgery. IPCAI'10, LNCS **6135** (2010) 23–33.

[6] K.T., Rajamani, et al.: Statistical deformable bone models for robust 3D surface extrapolation from sparse data. Medical Image Analysis, **11** (2007) 99–109.

[7] R., Hartley, and A., Zisserman: Multiple view geometry in computer vision.. 2nd Edition, 2004, Cambridge Univeristy Press.